



Non-Intrusive Flow Diagnostics for Aerospace Applications

L. Venkatakrisnan

Abstract | A brief account of several non-intrusive qualitative and quantitative visualization techniques used in aerospace research is presented. The broad principles of operation are described along with applications that are illustrative of their capabilities.

1 Introduction

The visualization and measurement of flows for understanding their physics and subsequent control have been the subject of innumerable investigations. This effort is aided by several kinds of measurement techniques. Broadly speaking, these techniques can be divided into intrusive and non-intrusive kinds. As is indicated by the term, non-intrusive methods have a significant benefit of being able to document a flow without interference from the measurement technique. As such, these methods should, in principle, be preferred over those that are intrusive. However, the development and application of non-intrusive methods remains challenging, more so in the context of aerospace applications where the flow regimes including very low and very high speeds are characterized by large and complex setups that can hinder application by both lack of optical access as well as harsh environments.

The non-intrusive flow diagnostic techniques can broadly be grouped into three types: surface flow visualization, scattering from flow tracers, and density sensitive flow visualization. These can either be of qualitative or quantitative type. While qualitative techniques need careful interpretation, very often they yield insight in to the physics of the flow. These fall in the broad category of flow visualization and will be referred to as such for the purpose of this paper.

Most quantitative techniques provide qualitative data in addition to quantitative data. A large number of these are laser and image based. These again can be point measurements or full-field measurements. Very often the resolution of the data available is limited by the capacity of the imager or the ability to illuminate the flow field. Great many techniques exist, these include, but

are not limited to: surface visualization using oil flow, wall tufts, chemical sublimation, off-body visualization by smoke flow, dye flow, hydrogen bubbles, speckle photography, density changes, laser induced fluorescence, measurement by oil film skin friction measurement, particle image velocimetry, laser Doppler velocimetry, pressure sensitive paints and interferometry.

The following sections will attempt to describe a few techniques that have been used to enhance flow physics understanding and the improvements to existing techniques carried out by the author and his colleagues at the CSIR-National Aerospace Laboratories, Bangalore.

These techniques are presented in the sections below with brief outlines of their operating principles and demonstration of their capabilities with examples of applications to aerospace flows.

2 Flow Visualization

Flow visualization is one of the most effective tools in flow analysis. It has helped immensely in elucidating basic fluid mechanics principles and in understanding complex fluid flow. Flow visualization makes visible a property of a flow field to facilitate better observation, and therefore analysis of a phenomenon. Normally, most fluids, either gaseous or liquid, are transparent, and therefore, invisible to the eye unless a special technique to render them visible is applied. Several flow visualization techniques have been developed for routine application in wind/water tunnels.¹

2.1 Surface flow visualization

Surface flow visualization plays an important role in understanding of flow physics by visualization of the flow pattern very close to the body surface. Typically, in this method, the surface is coated

*Experimental Aerodynamics
Division, CSIR, National
Aerospace Laboratories,
Bangalore, India, 560017.
venkat@nal.res.in*

with a thin layer of a material, which upon the interaction with the fluid flow develops a certain visible pattern. This pattern can be interpreted qualitatively, and in some cases, it is even possible to deduce quantitative data of the state of the flow close to the surface.²

2.1.1 Oil flow visualization: The surface oil flow technique is perhaps the most routinely used surface visualization method. In this qualitative method, a suitable oil is mixed with a pigment and sprayed to form small dots on the test surface. Shearing force in the flow acts on the oil, which moves in the direction of the surface velocity vector. The pattern so formed shows the flow direction on the surface of the model and can reveal transition, separation, and secondary flow patterns.³ Advantages of the method are that it is non-intrusive, can be used for any steady flows, and the flow direction can be observed during the run; the patterns may be photographed either during or after the run, and the results are usually recorded in the form of still photographs resulting in data in the form of images.

Many instructions have been given in literature on how to prepare an oil-pigment mixture appropriate for specific test conditions⁴ (e.g., Settles and Teng, 1983). However, in actual practice, it still remains a trial and error approach to find the right consistency such that it will run easily enough under the given test conditions and leave behind the streaks of pigment indicating the direction of flow.

Usually the surface flow visualization is carried out using a mixture of oleic acid, titanium dioxide powder and SAE 60 grade vacuum pump oil in

the ratio of 1:5:7. The mixture was sprayed on to the model by means of repeated flicking of the bristles of a paint brush till the model was covered with uniform sized discrete dots of a size that did not move under the influence of gravity. The oil streaks generated by the air flow give a better impression of the flow direction, and the method then is independent of the appropriate form of coagulations of the pigment.¹

Figures 1a and b show images from surface oil flow visualization on a typical Micro Aerial Vehicle (MAV),⁵ depicting the effect of the propeller wake on the flow over the vehicle. The asymmetry that such vehicles commonly exhibit when at large incidences (here 24°) and low speeds (10 m/s), is demonstrated in the image on the left (propeller off) and the restoration of symmetry due to the propeller wake, which dominates the flow behavior is shown on the right. The images demonstrate the depth of understanding that can be obtained from a simple visualization experiment.

It is to be noted here that the body under consideration is majorly two-dimensional; hence the images are a true representation of the flow. An image is the result of a perspective projection of a three-dimensional (3D) object to two dimensions (2D). As long as the model surface is largely 2D as in the previous example, this approximation suffices. It has long been recognized⁶ that the construction of three dimensional surface fields is an extremely difficult task, largely due to the fragmented nature of information (2D images). Delery⁶ suggests that to arrive at a rational construction, this fragmentary information must be complemented by a large dose of imagination with the guide of

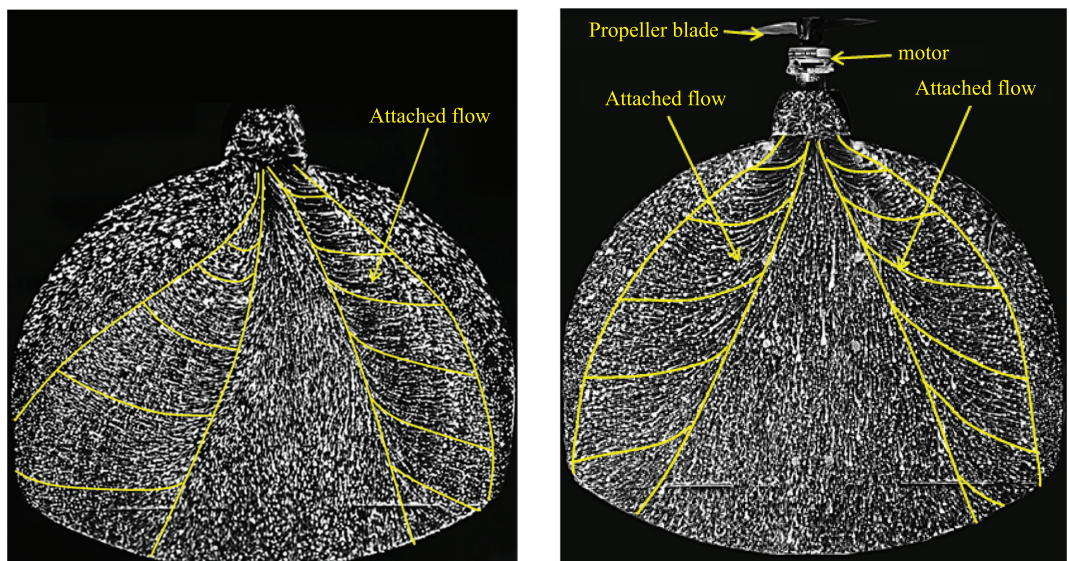


Figure 1: At $U_\infty = 10$ m/s (a) Propeller-off; $\alpha = 24^\circ$; (b) Propeller-on; $\alpha = 24^\circ$ (From [5]).

logical rules, and the capacity to see objects in three dimensions. This is demonstrated by the visualization images of flow over a landing gear at low speeds in Figure 2.

The images show the documentation of all the complex flow features including separation, reattachment, focus, saddle points, which are expected for a highly three-dimensional flow such as the present one. This renders the task of reconstructing flow topology rather challenging. Venkatakrishnan and Karthikeyan¹ proposed a method of photogrammetric resection based on a comprehensive camera model to map oil flow visualization images on to the surface grid of the model. The result of this is shown in Figure 3. The data that is exported in the VRML format allows for user interaction in a manner not possible with two-dimensional images. The format has the added advantage of being able to obtain the precise location of flow features resulting in extraction of quantitative data from a predominantly qualitative technique.

2.1.2 Tuft flow visualization: One of the main disadvantages of the oil flow visualization technique is that it cannot be used for unsteady flows. In such cases, the tuft flow visualization technique is appropriate. The primary objective in tuft flow visualization is to visualize the instantaneous flow

direction indicated by tufts. Being qualitative, it helps flow analysis in the following way: when the flow becomes unsteady or turbulent, the tufts perform a certain unsteady motion, and this may be taken as an indication that the wall boundary layer has become turbulent. More violent motion of the tufts or a tendency to lift from the surface, may indicate a separated flow regime. The choice of tuft size and material depends on the flow conditions and the size of the model to be tested.⁷

Woolen strand is an ideal material for the tuft as it is thick, flexible and bright coloured. Silk strands may be used in small scale low speed measurements. Fluorescent mini-tufts illuminated by UV light have also been used.⁸

The tuft method has been used in NAL on application to studying the flow on micro-aerial vehicles by Mukund and Karthikeyan.⁹ The tuft flow pattern in Figure 4a shows the tufts near the trailing edge directed upwards indicating reverse flow in the region.

The random tufts from the leading edge to the mid-chord region indicate separated flow. For another flow condition, Figure 4b, there is a clear reattachment line between the reverse flow upstream and attached flow downstream, showing that there is a separation bubble extending over most part of the chord, followed by attached flow.

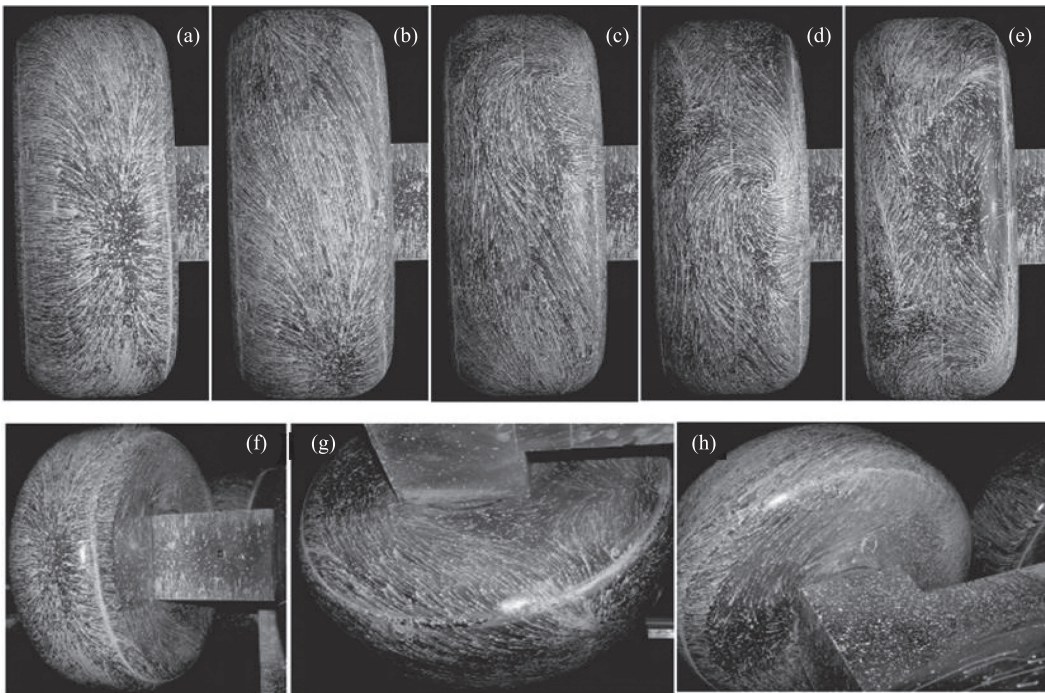


Figure 2: Front wheel of landing gear model imaged at various at (a-h) different azimuthal positions and (f-h) perspective views. Images are for wheel rotated by (a) 0° (b) 50°, (c) 100°, (d) 150°, (e) 200°. Perspective views: (f) Front half, (g) Bottom half, (h) Top half. (Adapted from [1]).

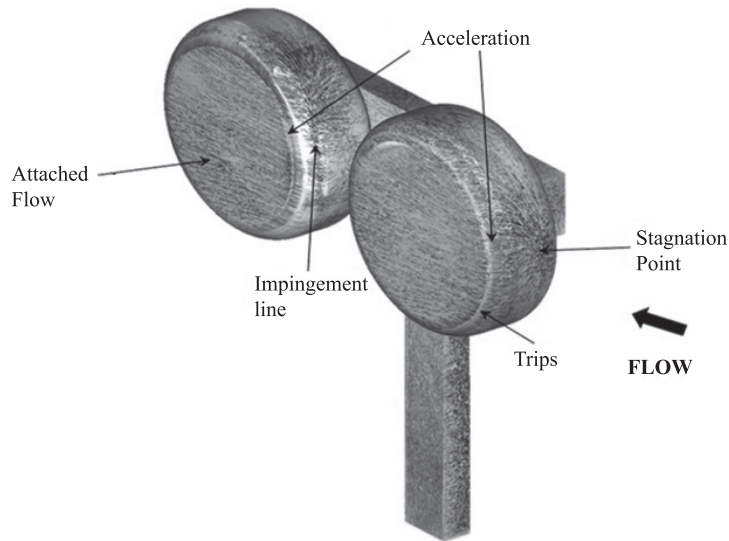


Figure 3: Landing gear model (one half) with texture mapped oil flow visualization data (From [1]).

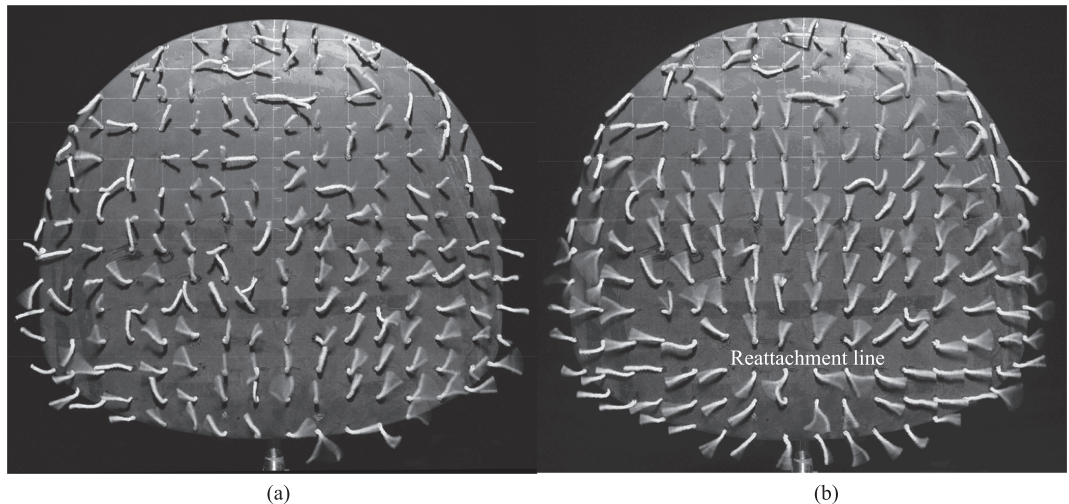


Figure 4: Tuft flow visualization on an MAV model in (a) fully separated condition and (b) with a large separation bubble (From [9]).

The images have to be taken during flow. The disadvantage of the method is that gross tufts may disturb the boundary layer and alter the flow downstream.

2.1.3 Shear sensitive liquid crystal technique:

The flow over a surface, in order to adjust itself to the no-slip condition at the surface, involves a boundary layer near the wall. The primary mechanism of the turbulent boundary layer lies in its ability to convert free-stream momentum into a shear force acting over the surface. The measurement of the shear stress at the wall for wall-bounded flows is of enormous importance for both theoretical and practical reasons. The

skin friction coefficient is a measure of this capacity (per unit surface area) as it constitutes the ratio of the mean wall shear stress to the axial free-stream momentum flux per unit area.¹⁰ The design of streamlined vehicles (e.g. aircraft and submarines) requires the accurate prediction of this coefficient.

The shear sensitive liquid crystal (SSLC) technique achieves this by means of coating the surface with a chemical that undergoes transient color changes that result from the change in pitch of the helix of its cholesteric structure due to change in mechanical stress. While obtaining quantitative shear stress information using color as a parameter for measuring both the magnitude

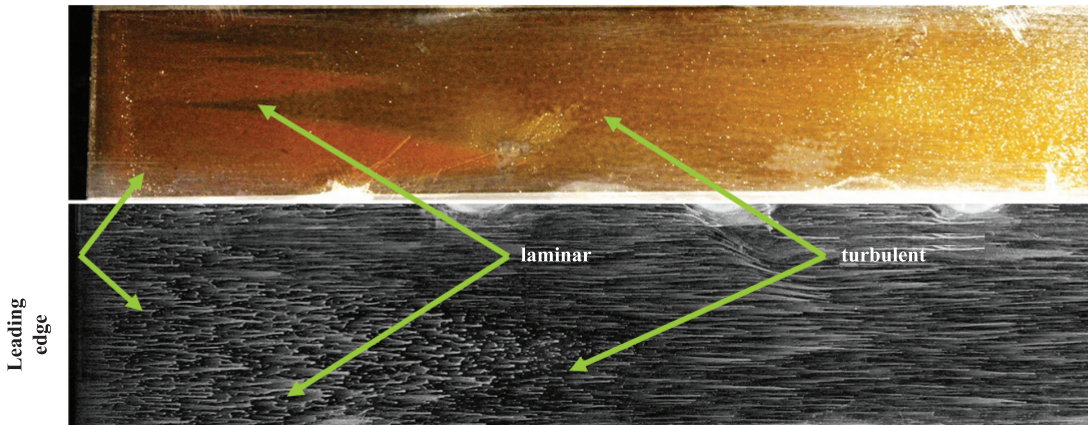
and direction of a skin friction vector can be formidably difficult, considerable qualitative information can be obtained without calibration, as is shown in the following applications.

Figure 5a shows the result of an attempt¹¹ to detect flow transition from laminar to turbulent flow over a flat plate model for Mach number of 2.5 in the 0.3 m trisonic wind tunnel at CSIR-NAL. The model is coated along its length with SSLC (Hallcrest, CN/R2) to a thickness of 20 μm . Figure 5a shows a comparison of SSLC and oil flow visualization images, clearly identifying transition wedges, followed by the turbulent boundary layer. Location of the wedges is different in both cases due to the presence of microscopic disturbances. The visualization also identified a mild but progressive change in the color in the turbulent boundary layer, implying that the increasing shear stress can also be resolved.

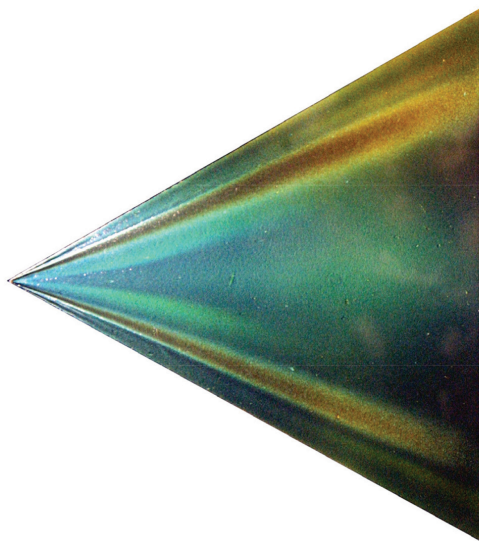
Figure 5b shows another application on a 60° delta wing model conducted at $M_\infty = 0.3$ and incidence of 10° in the same tunnel. The model was coated with SSLC Hallcrest CN/R3. The figure clearly shows footprints of primary and secondary vortices as well as of the attached flow region. The image shows several flow regimes with gradations in intensity. A pre-calibration of the SSLC would yield useful information on the shear field.

2.1.4 Pressure sensitive paint technique:

Surface pressure measurements are of great importance for basic fluid dynamics experiments, studying specific flow phenomena, and validating computational fluid dynamics codes. The surface pressure measurements are routinely carried out to investigate and measure aerodynamic parameters and provide inputs to structural designers, the data that is crucial during initial design cycle.



(a) Detection of transition on the flat plate using SSLC and oil flow visualization techniques



(b) Flow visualization using SSLC on a delta wing at $M_\infty = 0.3$, $\alpha = 10^\circ$

Figure 5: Flow visualization using Shear Sensitive Liquid Crystals (SSLC) (From [11]).

The Pressure Sensitive Paint technique (PSP) is a method that provides quantitative surface pressure on the test article under investigation. The PSP method is based on the property of photoluminescence of certain organic compounds. The article is sprayed with PSP and excited by UV light and luminescence emitted is captured using a CCD camera¹² (Fig. 6).

The calibration of luminescence intensity yields pressure distribution on the model. The technique provides both flow visualization and quantitative pressure data.

The PSP data reduction process, which transforms intensity data in the image plane into pressure data mapped to spatial coordinates of the model using a model grid, is an important element in the accuracy that can be achieved by the method. This is achieved by forming the ratio

of the wind-on pressure sensitive images by wind-off pressure sensitive images, each normalized by their reference images to correct for non-uniform illumination. Because there are two cameras for a binary paint and the models may get slightly displaced and deformed under wind loads, the images have first to be registered or transformed so that when the images are laid over each other, the corresponding physical points of the model are in alignment.^{13,14} The technique can be used to document both steady as well as unsteady pressures on the model surface. The latter, termed Fast PSP, however, is currently limited to a few kHz.

The capability of the system to generate data on complex aircraft configurations is demonstrated here on a 1:20 scale model of a fighter aircraft at freestream Mach numbers of 0.5 in the 1.2 m wind tunnel at CSIR-NAL. Figure 7 shows a PSP map

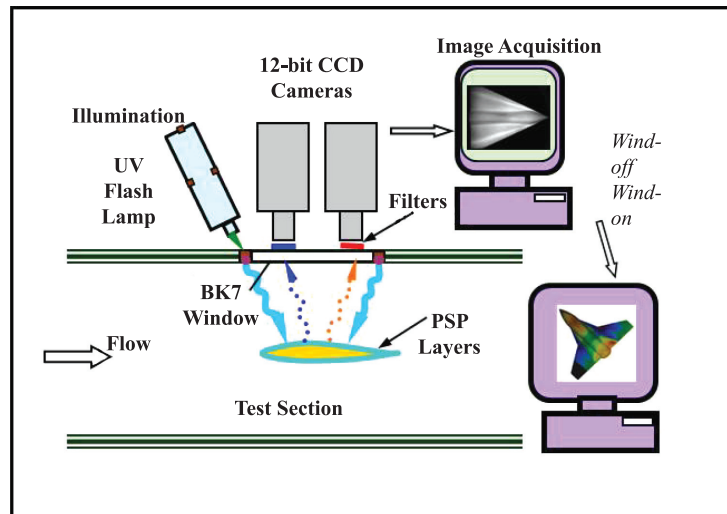


Figure 6: Principle of operation of PSP technique (Adapted from [12]).

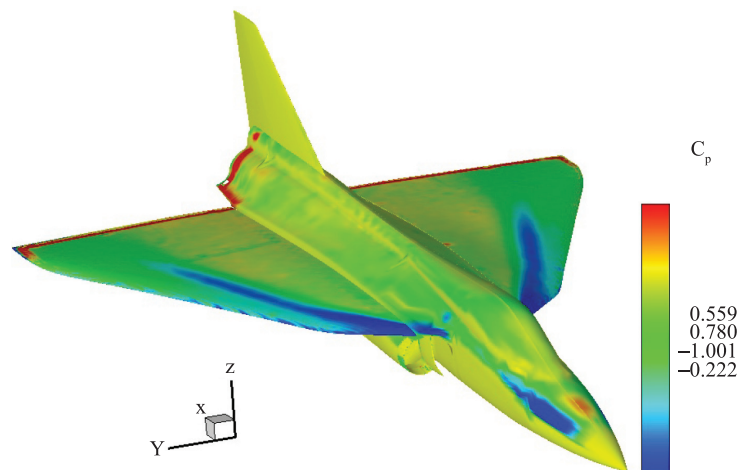


Figure 7: PSP map on the leeward side of a fighter aircraft showing flow features and quantitative data.

of the steady pressure field on the lee side of the model; the figure shows a map of the distribution of pressure in terms of a coefficient of pressure. The map shows clearly the regions of low pressure (indicated by the blue regions) in the primary vortices over the delta wings as well as around the forebody and a zone of higher pressure at the nose below the cockpit facing the flow. The data show the incredible resolution enabled by the technique, limited only by the resolution of the sensor, as opposed to discrete measurements allowed by conventional methods such as pressure taps.

An excellent review of steady pressure sensitive paint technology and applications is provided by Gregory et al.¹⁵ The status of fast PSP is reviewed by Gregory et al.¹⁶

2.2 Off-body flow visualization

2.2.1 Schlieren: When the flow of interest is characterised by a change in the density, often due to the effect of compressibility of the fluid, the change in refractive index can be exploited to reveal the behavior of the flow. The technique that renders such flows visible is termed the Schlieren technique.

Schlieren (from German; singular “schliere”) are optical inhomogeneities in transparent material not visible to the human eye. Schlieren physics developed out of the need to produce high-quality lenses devoid of these inhomogeneities. These inhomogeneities are localized differences in optical path length that cause light deviation.

Schlieren flow visualization is based on the deflection of light by a refractive index gradient. The index gradient is directly related to flow density gradient.¹⁷ As shown in Fig. 8, a ‘point’ light source (S) is collimated by a first lens, whose focal point coincides with the location of the source. Then the parallel light rays pass through the test section and a second lens refocuses the beam to an image of the point source. Transparent Schlieren objects are not imaged at all until a knife-edge is added at

the focus of the second lens. The deflected light is compared to un-deflected light at a viewing screen. The undisturbed light is partially blocked by a knife edge. The light that is deflected toward or away from the knife edge produces a shadow pattern depending upon whether it was previously blocked or unblocked. This shadow pattern is a light-intensity representation of the expansions (low density regions) and compressions (high density regions), which characterize the flow. For this particular point of the Schlieren object, the phase difference caused by a vertical gradient in the test section is converted to an amplitude difference and the invisible is made visible.

A word about the orientation of the knife-edge: here (in Fig. 9) shown horizontal, it detects only vertical components in the Schlieren object. That is, a simple knife-edge affects only those ray refractions with components perpendicular to it. If the gradients in the Schlieren object are mainly horizontal, then the knife-edge should be placed vertically in the focus of the second lens.

Figure 9 shows a Schlieren image (horizontal knife-edge) of supersonic flow ($M_\infty = 2$) over an elliptic cone at 10° angle of incidence along the minor axis plane.¹⁸ The shock waves subtended at the tip of the cone are seen and allow measurement of shock angles. This data can be used in isentropic flow relations to obtain information about the strength of the shock. While this particular example is of steady flow, shorter duration exposures by means of either spark light sources or high framing cameras can be used to capture unsteady behavior.

Figure 10 shows an application¹⁹ to flow past the afterbody (tail region) of an aircraft. The instantaneous Schlieren image captures the unsteady shock-induced separation of the boundary layer as well as the turbulence in the wake.

The Schlieren technique has been used in a variety of situations, not confined to aerospace

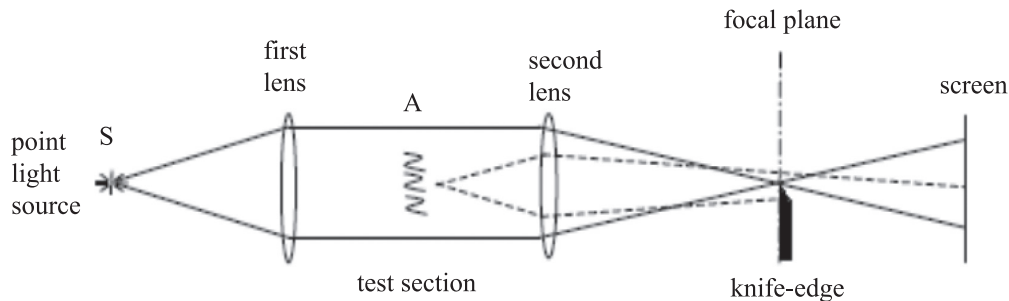


Figure 8: Schematic of a simple Schlieren system (From [17]).

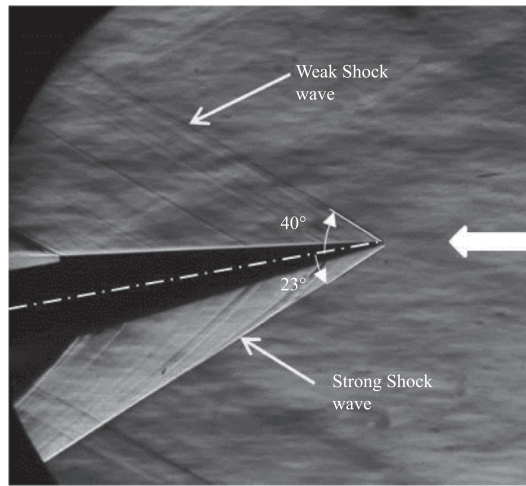


Figure 9: Supersonic ($M = 2$) flow over an elliptic cone viewed in the minor axis plane (From [18]).

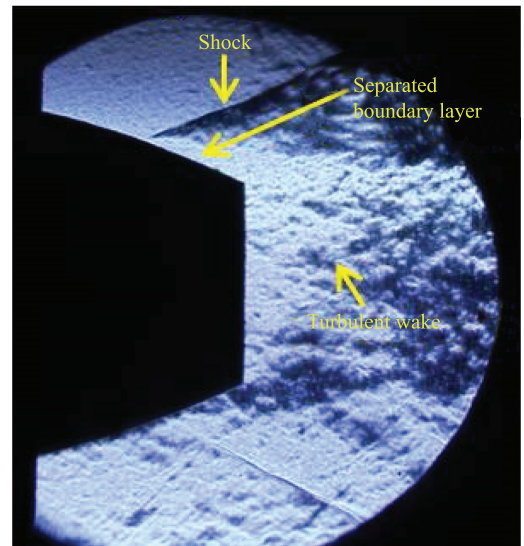


Figure 10: Instantaneous Schlieren image at $M_\infty = 1.34$ for jet-off condition showing maximum upstream location of shock (From [19]).

applications. Settles¹⁷ has documented great many variations of both the technique as well as its applications. Variations include laser Schlieren, Color Schlieren, short duration and high speed Schlieren and large scale Schlieren. Applications range from visualization of a fired bullet to thermal plumes from ovens or people to very large scale to visualize the shocks around a fighter aircraft in flight using the sun as a light source. Settles¹⁷ provides an excellent in-depth treatment of the subject.

2.2.2 Background oriented schlieren: The Schlieren technique, while exceedingly useful, is limited by its qualitative nature. Attempts to make quantitative estimates of density using calibration have been found to be exceedingly cumbersome. There have been several efforts at quantifying the density gradient field using either the 'Synthetic Schlieren' method^{20,21} or the 'Background Oriented Schlieren' – BOS.²² The synthetic Schlieren has been successfully used for measuring amplitudes of waves generated by an oscillating^{20,21,23} cylinder. And an oscillating sphere²⁴ in a stratified flow. The Background Oriented Schlieren, which is a quantitative Schlieren technique, is based on the principle that the image of an object is the convolution of the object function and the transfer channel function. Thus, a de-convolution will describe the transfer channel function if the object and image are given. A major advantage of this technique is that it requires only a digital still camera with adequate resolution and an appropriate background and yields quantitative density field data.

The principle of the technique is the refractive index variation due to density gradients in the flow

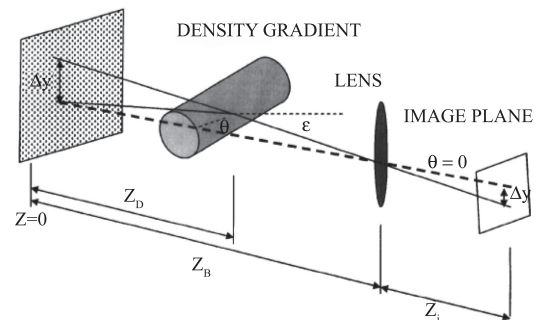


Figure 11: Optical path for density gradient measurements by light deflection (From [25]).

(Figure 11). The determination of the density field using BOS thus involves the following steps: a) Calculation of displacements in the background, which is imaged through the flow of interest. This is done through a PIV-type cross-correlation algorithm. These displacements are the vectors of density gradient at each point; b) Calculation of the line-of-sight integrated density field by solution of the Poisson equation, which is the gradient of the above displacement; c) Use of optical tomography (filtered back-projection) to determine the density field in the actual plane of interest.

Validation of this technique was carried out by applying BOS to obtain the density field for an axisymmetric supersonic flow over a cone cylinder model. Comparisons with cone tables showed excellent agreement. Venkatakrisnan and Meier²⁵ validated the BOS technique combined with filtered back-projection tomography, which

provides the mean density field in a 2D plane. The extraction of a desired plane using Filtered Back Projection Tomography was carried out by Venkatakrishnan.²⁶

Figure 12 shows the density field around an elliptic cone¹⁸ under the same conditions as in Figure 9. The image that is shown in a cutaway fashion to illustrate the capability of the technique to document the density field exhibits flow features of the shock wave from the tip and the density field around the body.

Application of BOS to an extremely short duration and spatio-temporal evolving flow field of a micro-explosion was carried out by Venkatakrishnan et al.²⁷ The complex nature of the chemical reaction process and spatial and temporally varying flow field in explosions impose serious limitations on applied diagnostics. The explosion is created by initiation of detonation inside a Nonel[®] tube by means of a spark and generates a wave front. This wave front compresses the air, which results in the formation of multiple compression waves coalescing to form a strong shock that expands into a spherical blast wave. Figure 13 shows the reconstructed density fields obtained using the BOS technique at different instants of time during the evolution of the blast wave. The data show the complexity of the flow, characterized by supersonic vortex rings, barrel shocks and a jet plume.

Such three-dimensional reconstruction of the density field is not possible by any other technique. The results clearly demonstrate the capability of BOS in visualizing and quantifying complex density fields.

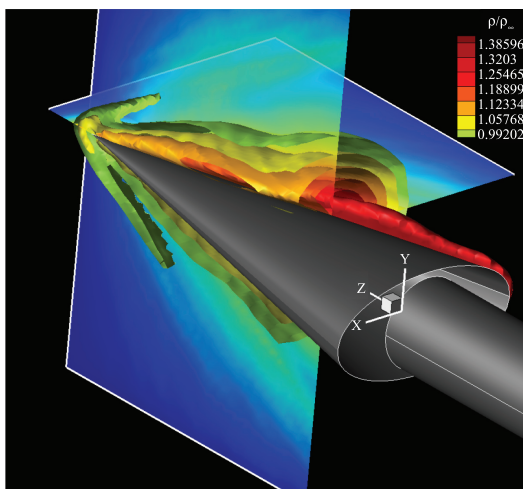


Figure 12: BOS generated density field of $M_\infty = 2$ flow over elliptic cone at incidence (From [18]).

The BOS technique has been applied to a large variety of flows, from the micro-explosions and wind tunnel applications described above to nozzles,²⁸ microjets,²⁹ full-scale helicopters in flight³⁰ and full-scales.³¹ These applications have spawned a number of variants of BOS including Coloured Grid BOS (CGBOS), Retroreflective BOS (RBOS), Natural Background BOS, and Pulsed illumination BOS. A comprehensive review can be found in Raffel.³²

2.2.3 Dye flow visualization: The visualization of water flows is usually accomplished by means of dye. The dye chosen has to fulfil requirements of neutral buoyancy, high stability against mixing and good visibility. They have to be non-toxic and include color as a means for elucidating flow patterns. If the mixture is not a true solution, under the action of inertial or centrifugal forces acting in different ways on components of the mixture, dye tracers might not indicate the true flow direction. Such discrepancy is avoided by complete dilution of the dye in water (food coloring, ink).⁷

A common technique of releasing the dye into the flow is through dye ports or slits, which are usually fabricated as part of the model. While deciding locations of the ports or slits, one must bear in mind that dye-lines are streaklines, and streaklines only display a spatially integrated view of the flow structures. This is because the dye distorts as it travels downstream; accordingly, the streakline pattern seen at some distance downstream of a test-model is a result of the accumulated distortion that can be traced all the way back to the point of release. In other words, the streakline pattern at a given location is a function of the location where the dye is released. Also, when releasing dye through dye ports, one must ensure that its exit velocity is kept to a minimum since a large exit velocity can significantly alter the flow behavior. Moreover, if dye is intended to mark vorticity, it must be released at the location where the vorticity is generated.

Figure 14 shows images from dye flow visualization experiments that were conducted in the CSIR-NAL water tunnel on an MAV planform without a camber.⁹ The flow velocity was 7.4 cm/s, and the chord Reynolds number = 10000 at an incidence of 25°. The figure shows the front view of the experiments with dye injected from top central port and two pairs of ports from the side. The figure clearly shows the leading edge separation, which is reattaching in the midchord region. Inside the laminar separation bubble, a nearly dead air region very close to the leading

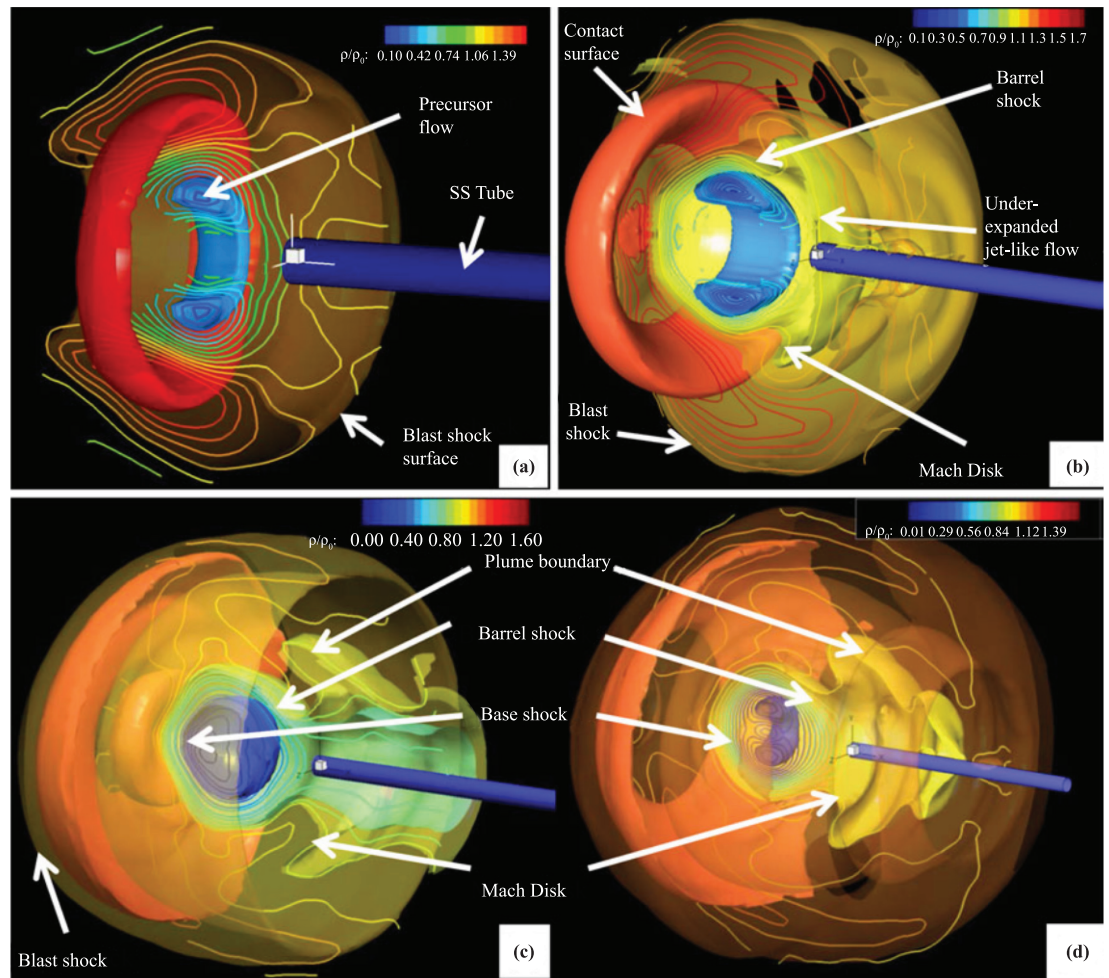


Figure 13: Reconstructed density field at (a) $t = 24 \mu s$, (b) $t = 53 \mu s$, (c) $t = 93 \mu s$ and (d) $t = 122 \mu s$ (From [27]).

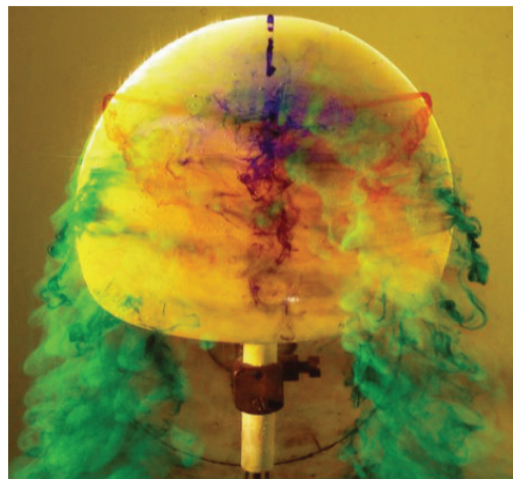


Figure 14: Dye flow visualization experiments in the water tunnel on MAV platform (From [9]).

edge and reverse flow beyond was observed. All these observations confirm those from the oil flow patterns. The front view identifies the extent and the shape of the laminar separation bubble and the shedding of strong tip vortices, which possibly help in the reattachment of the separated flow.

3 Flow Velocity Measurement Techniques

Measurement of the velocity field of a flow using intrusive probes always carries with it the possibility of interference with the flow, and thereby influence over the quantity it seeks to measure. Laser based techniques have provided a way to make non-intrusive measurements of the three-component velocity by usage of a seed in the flow to scatter the laser light. Care must be taken though to ensure that the chosen seeding fulfils the needs of neutral buoyancy and Stokes drag to follow the flow with fidelity.

3.1 Laser doppler velocimetry

Ever since the invention of laser in 1958, there have been rapid developments in many scientific and engineering applications of this phenomenal tool. One of the remarkable applications of laser for flow measurements has been the Laser Doppler Velocimeter (LDV). Laser Doppler Velocimeter, as the name indicates, is an instrument that performs measurement of velocity of a fluid, based on the famous Doppler-Fizeau effect. The fluid velocity is measured by measuring the velocity of micron-sized particles, present in the fluid, naturally occurring or by seeding.

Modern LDV systems have the capability for applications in a wide variety of flows under different situations: low speed flows to supersonic flows, natural free convection, internal flows, steam and gas turbines, reacting flows, atmospheric flows, high temperature plasmas and many others. The large number of applications of the tool is mainly due to its advantages of being non-intrusive, able to sense flow direction, free of calibration, highly spatially resolvable, insensitive to temperature effects. Using the concept of phase-Doppler analysis (PDPA), applications to particle size measurements are possible.

The power of the LDV technique is shown here in documenting the broad flow features of a typical airblast atomizer (used in gas turbines) in order to understand the flow physics of the spread and mixing processes that are extremely important for high combustion.³³ Figure 15a shows the exit details of the atomizer. Highly swirling air is used to atomize a pre-filmed layer of water (as surrogate fuel). Figure 15b and c depict streamwise mean velocity field obtained in the absence and presence of water. The contours of velocity are plotted both in color and as heights above the plane. The figure shows that the mean velocity field is not symmetric and has significant

circumferential variation of streamwise velocity towards the periphery, and that the velocity in the central core is strongly negative due to strong toroidal recirculation produced by the swirl. The exercise shows the kind of detailed analyses that can be carried out even in a complex two-phase flow with data using the LDV technique. Adrian³⁴ carries out a review of the LDV technique and compares it to other multipoint techniques.

3.2 Particle image velocimetry

One of the serious limitations of the LDV technique is that it is a pointwise measurement. This, in addition to the increased time required to map the plane of a given flow field, also implies the inability to carry out spatial correlations of data recorded simultaneously at different spatial locations; this is imperative for resolving non-stationary flow structures. Particle Image Velocimetry (PIV) technique is one answer to the challenge. The measurement of the velocity field using PIV is based on the ability to accurately record and measure the positions of small tracers suspended in the flow as a function of time.³⁵ The velocity is then deduced as the displacement divided by the time interval (Figure 16). The degree of closeness of this estimate to the true velocity depends on how accurate the particle displacement is measured and on the time interval. Too short interval an results in an undetectable displacement, whereas a too long intervals average out the fast fluctuating components.

Thus, for an accurate representation of the flow velocity, the time interval must be of the order of a relevant flow time scale. Typically, this scale is the ratio between the flow length scale, e.g., the Taylor macroscale, and the maximum velocity in the field. It is important to realize that once the ‘averaging’ time has been determined, the flow scales that are represented by the recorded images have been

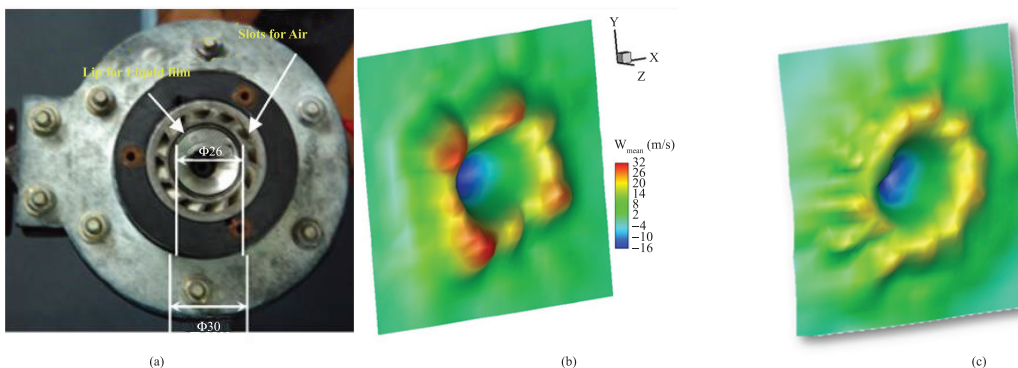


Figure 15: (a) Pre-filming atomizer; streamwise mean velocity field at 45mm from exit for (a) air-alone and (b) air-water cases (From [33]).

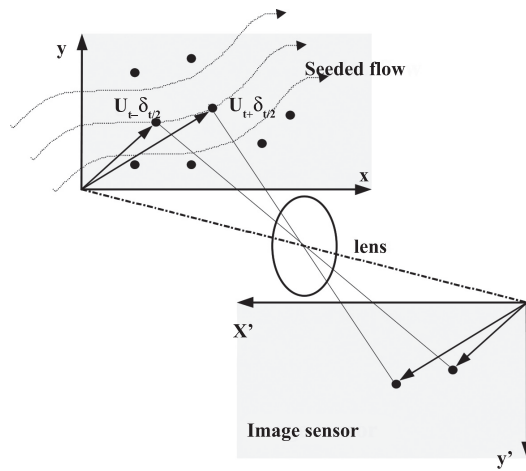


Figure 16: Principle of Particle Image Velocimetry (From [35]).

fixed, and information contained in time scales beyond the time interval are forever lost.

3.2.1 Two-component Particle Image

velocimetry: The tracer particles are illuminated by means of a thin light sheet generated from a pulsed light source (usually a double-head pulsed laser system), and the light scattered by them is recorded onto two subsequent image frames by a digital imaging device, typically a CCD camera. Correlation then yields the displacement of particles at each 'grid point' on the image. Figure 17 shows a cartoon of the process. Two dimensional PIV (2DPIV) enables the capturing of instantaneous and mean flow fields in a 2D plane of the flow illuminated by a laser. The velocity vector field so obtained can also be used to compute the vorticity fields. PIV has been applied to study subsonic and supersonic flows, as well as flows at extremely low speeds and water flows.

Application of 2D PIV can either be in an ensemble averaged form or be time-resolved (wherein the framing is faster than the flow time scales) or phase locked (i.e., capture the different phases of a periodic flow). Figure 18, which shows the mean velocity and vorticity field in the mid-plane of the vortex shedding behind a circular cylinder at low speed, demonstrates the latter. The trigger for the phase locking was achieved by means of a signal from a hot-wire probe, placed in the flow behind the cylinder. The reversed flow is indicated by red vectors. The presence of the shed vortex on the lower side of the cylinder, and vortex being formed on the top are clearly seen in the velocity and vorticity maps. The complex nature of the velocity field including reversed flow

zone may be observed, showing the asymmetric nature of the shedding from the upper and lower surfaces.

Application of PIV to high-speed supersonic flows, presents certain challenges. One of these challenges is associated with the inertia of particles used as scatters in the flow. Supersonic jet flows for instance, (unless ideally expanded) contain shock cells through which the flow accelerates and decelerates rapidly. Therefore, particles with larger mass and smaller slip drag cannot follow the flow with adequate fidelity. Particles of sufficiently small (usually sub-micron) diameters need to be used. Figure 19 shows the application of 2DPIV to a supersonic jet. The figure shows the mean velocity vector field as well as the vorticity field. The clustering of vectors also serves as a visualization of the shocks present in the jet flow field. The data is both immediately qualitative as well as quantitative and demonstrates the capability of PIV to capture supersonic flow fields.

The 2D PIV technique is now routinely applied in major wind tunnels globally with specialized adaptation developed to cater for the special requirements of each facility. A comprehensive documentation of such applications can be found in Stanislas et al.³⁹

3.2.2 Three component particle image

velocimetry: Out-of-plane motion (i.e., three-dimensional motion) of seeding particles that move out of the laser sheet plane is a severe limitation of 2D PIV in application to fluid flow. The reason for this limitation is that out-of-plane motion results in correlation loss. However, the fact that there is a detectable effect due the out-of-plane component of motion opens the possibility for its measurement. The strategy consists of a stereoscopic technique capable of measuring three velocity components in selected planes of a flow field. The technique is flexible enough and especially adapted for use in Wind Tunnel Applications. In this method, the images of particles suspended in the flow are recorded using a stereoscopic set-up. The stereo-pair views of the 'flow-plane' are acquired in digital form via a high-resolution electronic imager. Each stereo-pair view is processed using a high-resolution correlation algorithm yielding velocity maps that are combined to reconstruct the three-dimensional velocity field. Due to the off-axis viewing of the laser plane, a special lens mount called a Schiemplug mount (Figure 20) is used to avoid de-focus of the plane on to the sensor array.

StereoPIV was employed to study⁴⁰ the axis-switching phenomenon in a 2:1 elliptical jet with an

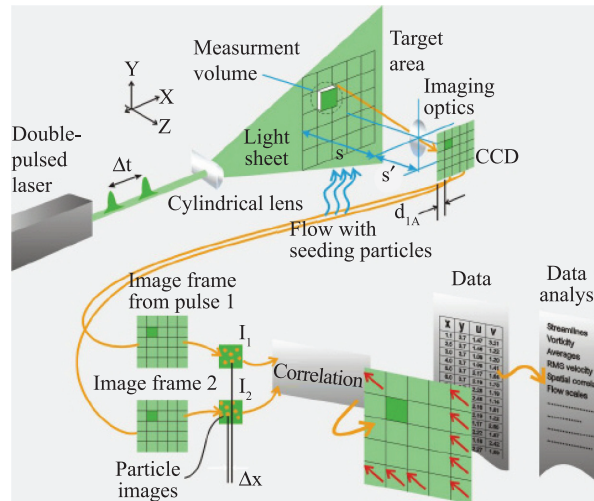


Figure 17: Schematic of a typical 2D PIV setup (From [36]).

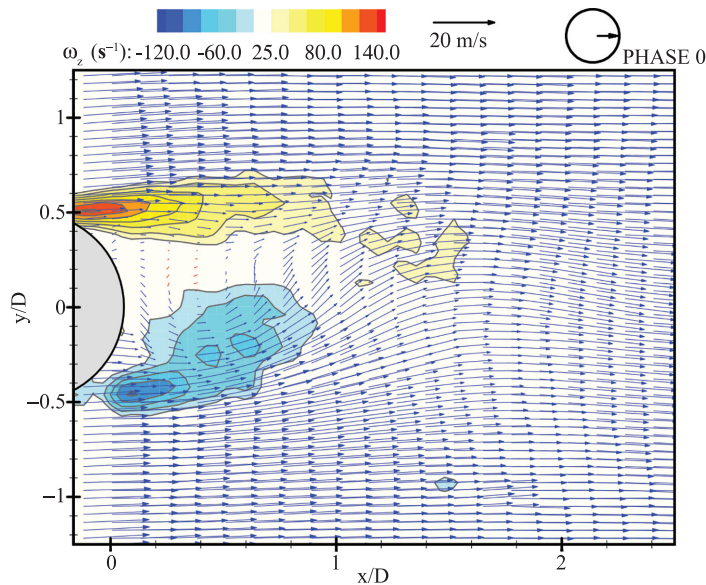


Figure 18: Phase-averaged velocity field at zero degrees (From [37]).

exit velocity of 22 m/s and $Re = 56000$ (V&GR). The objective was to document the flow field and determine the location of axis-switching. The contours of streamwise velocity at different axial stations showed that the axis-switching process (from vertical to horizontal) occurs over a zone and not at a single point as usually believed. Figure 21 shows the three-component field at the exit plane of an elliptic nozzle.

In order to further demonstrate the capabilities of StereoPIV in understanding flow physics, it is instructive to re-look at the MAV investigation referred to in Section 2.1.1. The surface oil flow visualization depicted an asymmetry in the

absence of propeller flow, which disappeared in the propeller-on condition. The same configuration at identical conditions was documented using StereoPIV at four cross-planes along the chord. Figures 22 a,b show the results of the exercise.⁴¹ The figure shows the vorticity at field at the first and last cross planes. The iso-surfaces of the vortex cores are also plotted, as are the streamtraces through the vortex cores. In the propeller off condition, the port side has higher magnitude of positive vertical velocity component in the tip; lower magnitude of negative vertical velocity component in the inboard region and lower magnitude of tangential velocity component near the surface compared to

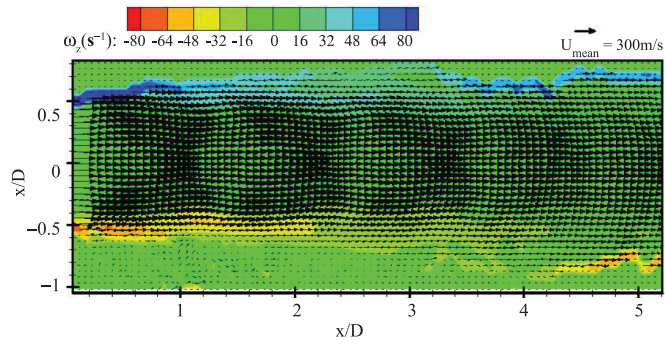


Figure 19: Mean flow field of the axisymmetric supersonic jet using PIV (From [38]).

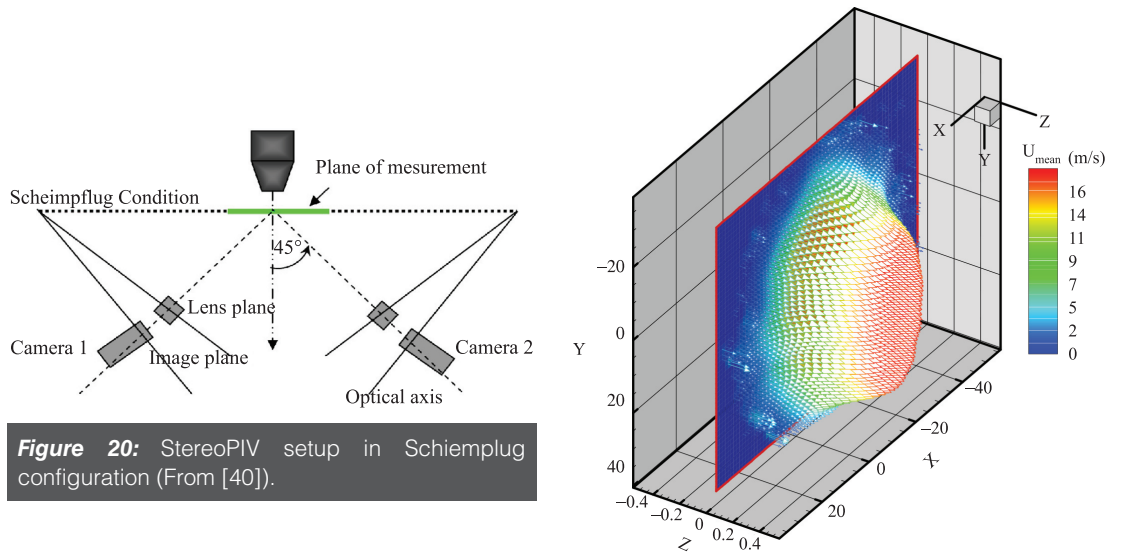


Figure 20: StereoPIV setup in Schiempflug configuration (From [40]).

Figure 21: Three-component velocity field at the exit plane of elliptic nozzle (From [40]).

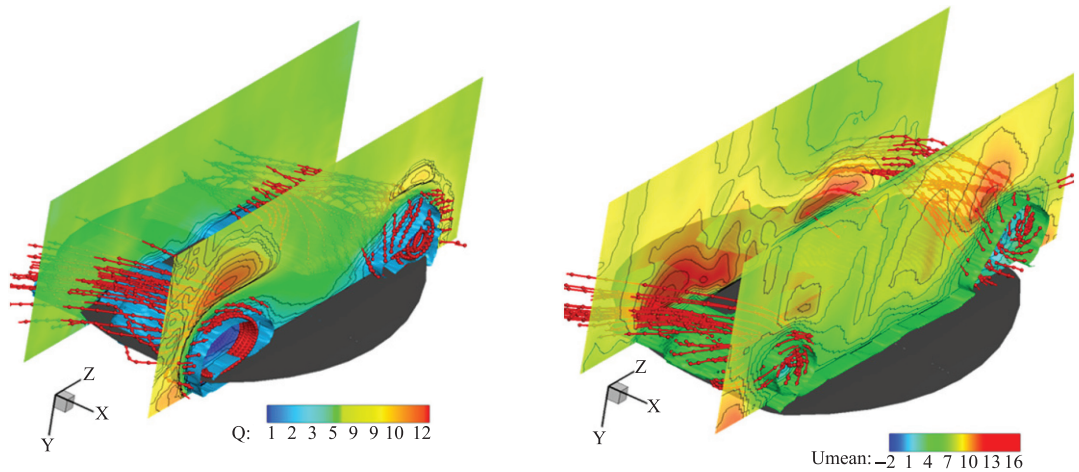


Figure 22: Three component velocity field over MAV at 24° incidence (a) Propeller Off and (b) Propeller On (From [41]).

the starboard side. Due to this, a weak signature of a vortex is seen in the oil flow visualizations at port side. This is well supported by the asymmetry in the streamtraces, and differences in vorticity contours between the port, and starboard side in the propeller-off condition. During prop-on, both tangential and vertical components are equal in magnitude on both sides of the wing centerline and the magnitude of the negative vertical velocity increased in the inboard region, which brings the flow towards the wing planform and causes the attached flow. These correspond to the flow pattern from the oil flow visualization.

4 Future Outlook

Non-intrusive measurement techniques have made a significant impact on measurement technology in aerodynamics. The capabilities of these techniques have received a fillip due to improvements in illumination, imaging sensor and computing capabilities.

The recent improvements in time resolved volumetric PIV, fast PSP, and BOS indicate that the goal of accurately measuring velocity, strain, density and pressure in 2D or 3D regions of a flow field, be it steady or unsteady, laminar or turbulent, compressible or incompressible is quite achievable. Further, the data, which are achieving resolutions hitherto not possible with conventional measurements, allow better understanding of flow physics.

Acknowledgments

The author would like to acknowledge all his co-authors who have contributed to the application examples shown here. He would also like to thank Dr R. Mukund and Dr Channa Raju, his colleagues at CSIR-NAL, for sharing their results.

Received 2 March 2016.

References

1. N. Karthikeyan and L. Venkatakrishnan, Application of photogrammetry to surface flow visualization, *Exp Fluids*, **50**, 689–700 (2010). doi:10.1007/s00348-010-0978-x.
2. W. Merzkirch, Flow visualization. Academic Press, London (1987).
3. A.J. Smits and T.T. Lim, Flow visualization – Techniques and examples. Imperial College Press, London, (2000).
4. G.S. Settles and H.Y. Teng, Flow visualization of separated 3-D shock wave turbulent boundary layer interactions, *AIAA J*, **21**, 390–397 (1983).
5. S. Sudhakar, Chandan Kumar, D. Arivoli, Ravi Dodamani, and L. Venkatakrishnan, Experimental Studies of Propeller Induced Flow Over a Typical Micro Air Vehicle, Paper AIAA 2013-0060, 51st AIAA Aerospace Sciences Meeting including the New Horizons Forum and Aerospace Exposition, Aerospace Sciences Meetings (2013). <http://dx.doi.org/10.2514/6.2013-60>.
6. J.M. Delery, Robert Legendre and Henri Werle: Towards the elucidation of three-dimensional separation, *Ann Rev Flu Mech*, **33**, 129–154 (2001).
7. W. Merzkirch, Techniques of Flow Visualization, AGARD-AG-302 Advisory Group for Aerospace Research and Development North Atlantic Treaty Organization ISBN 92-835-0438-0 (1987).
8. J.P. Crowder, Fluorescent minitufts for nonintrusive flow visualization, InFlow Visualization II: W. Merzkirch (editor), Washington, Hemisphere, pp. 663–667, (1982).
9. R. Mukund and N. Karthikeyan, Experimental investigations and evaluation of MAV planforms. NAL-PD-EA-0921 (2009).
10. Springer Handbook of Experimental Fluid Mechanics, C. Tropea, L.A. Yarin and J.F. Foss (Eds), ISBN: 978-3-540-25141-5 (2007).
11. K.T. Madhavan and R. Mukund, Transition Flow Visualization using Shear Sensitive Liquid Crystals at High Speeds. Project Document EA 0807, (2008).
12. C. Raju and P.R. Viswanath, Pressure-sensitive paint measurements in a blowdown wind tunnel, *Journal of Aircraft*, **42**(4), 908–915 (2005).
13. L. Venkatakrishnan, Comparative study of different pressure-sensitive-paint image registration techniques, *AIAA Journal*, **42**(11), 2311–2319 (2004).
14. C. Raju, L. Venkatakrishnan and P.R. Viswanath, Pressure Sensitive Paint measurements on a delta-wing in supersonic flow, *Aero J Roy. Aero. Soc.*, **110**, 767–771 (2006).
15. J.W. Gregory, K. Asai, M. Kameda, T. Liu and J.P. Sullivan, A review of pressure-sensitive paint for high-speed and unsteady aerodynamics, *Proc Inst Mech Eng Part G J Aerosp Eng*, **222**(2), 249–290 (2008). doi:10.1243/09544100.
16. J.W. Gregory, H. Sakaue, T. Liu and J.P. Sullivan, Fast pressure-sensitive paint for flow and acoustic diagnostics, *Annu Rev Fluid Mech*, 303–330 (2014). doi:10.1146/annurev-fluid-010313-141304.
17. G.S. Settles: Schlieren and Shadowgraph Techniques. ISBN 3-540-66155-7, Springer-Verlag, (2001).
18. L. Venkatakrishnan, P. Suriyanarayanan and J.S. Mathur, Measurement of three dimensional density field around an elliptic cone at Mach 2 using BOS technique, PDEA1203, (2012).
19. L. Venkatakrishnan and P. Suriyanarayanan, Density field of supersonic separated flow past an afterbody nozzle using tomographic reconstruction of BOS data, *Exp Fluids*, **47**(3), 463–473 (2009).
20. S.B. Dalziel, G.O. Hughes and B.R. Sutherland, Whole field density measurements by Synthetic Schlieren, *Exp Fluids*, **28**, 322–335 (2000).
21. B.R. Sutherland, S.B. Dalziel, G.O. Hughes and P.F. Linden, Visualization and measurement of internal gravity waves by ‘Synthetic Schlieren’. Part I. Vertically oscillating cylinder, *J Flu Mech*, **390**, 93–126 (1999).

22. M. Raffel, H. Richard and G.E.A. Meier, On the Applicability of Background Oriented Optical Tomography for Large Scale Aerodynamic Investigations, *Exp Fluids*, **28**, 477–481 (2000).
23. B.R. Sutherland and P.F. Linden, Internal wave excitation by a vertically oscillating elliptical cylinder, *Phys. Fluids*, **14**, 721–731 (2002).
24. K. Onu, M.R. Flynn and B.R. Sutherland, Schlieren Measurement of Axisymmetric Wave Amplitudes, *Exp Fluids*, **35**(1), 24–31 (2003).
25. L. Venkatakrishnan and G.E.A. Meier, Density Measurements using Background Oriented Schlieren Technique, *Exp Fluids*, **37**(2), 237–247 (2004).
26. L. Venkatakrishnan, Density Measurements in an Axisymmetric Underexpanded Jet Using Background Oriented Schlieren Technique, *AIAA J*, **43**(7), 1574–1579 (2005).
27. L. Venkatakrishnan, P. Suriyanarayanan and G. Jagadeesh, Density Field Visualization of a Micro-Explosion Using Background Oriented Schlieren, *J Vis*, **16**, 177–180 (2013). doi:10.1007/s12650-013-0164-3.
28. D.J. Tan, D. Edgington-Mitchell and D. Honnery, Measurement of density in axisymmetric jets using a novel background-oriented schlieren (BOS) technique, *Exp Fluids*, **56**(204), 1–11 (2015). doi:10.1007/s00348-015-2076-6.
29. R. Kumar, A. Wiley, F. Alvi and L. Venkatakrishnan, Role of coherent structures in supersonic impinging jets, *Phys. Fluids*, **25**, 076101 (2013). <http://dx.doi.org/10.1063/1.4811401>.
30. A. Bauknecht, B. Ewers, C. Wolf, F. Leopold, J. Yin and M. Raffel, Three-dimensional reconstruction of helicopter blade tip vortices using a multi-camera BOS system, *Experiments in Fluids*, **56**(1866), 1–13 (2015). doi:10.1007/s00348-014-1866-6.
31. M.J. Hargather, Background-oriented Schlieren diagnostics for large-scale explosive testing, *Shock Waves*, **23**, 529–536 (2013). doi:10.1007/s00193-013-0446-7.
32. M. Raffel, Background-oriented Schlieren (BOS) techniques, *Exp Fluids*, **56**(60), 1–17 (2015). doi:10.1007/s00348-015-1927-5.
33. P. Suriyanarayanan, N.S. Vikramaditya and L. Venkatakrishnan, Investigations of the air and liquid velocity fields in a prefilming airblast atomizer. Proceedings of the Indo-US Workshop on Spray Diagnostics, Dec 2011 Chennai, (2011).
34. R.J. Adrian, Multi-point optical measurements of simultaneous vectors in unsteady flow—A review. *Intl J Heat and Fluid Flow*, **7**(2), 127–145 (1986).
35. L. Lourenco, A. Krothapalli, and C. Smith, Particle Image Velocimetry, *Advances in Fluid Mechanics Measurements*, Ed: M. Gad-el-Hak, Springer-Verlag, pp. 128–199, (1989).
36. www.dantcdynamics.com.
37. L. Venkatakrishnan, K.T. Madhavan and P.R. Viswanath, Phase-Averaged 2D PIV Measurements on a cylinder with Forward Splitter Plate. Discussion Meeting on Flow Control and Diagnostics, 19–22 Feb 2006, Coorg, India, (2006).
38. L. Venkatakrishnan and N.B. Mathur, PIV Studies in Under Expanded Supersonic Jets, NAL PD EA 0610, May 2006.
39. Particle Image Velocimetry: Progress Towards Industrial Application, M. Stanislas, J. Kompenhans and J. Westerweel (Eds.)
40. L. Venkatakrishnan, Some Observations on the Axis-Switching Elliptic Jet. *Sym Adv Flu Mech*, July 24–25, 2003, Bangalore, India, (2003).
41. S. Sudhakar, Chandan Kumar and L. Venkatakrishnan, Influence of Propeller slipstream on vortex flow field over a Typical Micro Air Vehicle (*In Preparation*), (2016).



Dr. L. Venkatakrishnan obtained his PhD in Aerospace Engineering at the Indian Institute of Science in 1997, before joining the Fluid Mechanics Research Laboratory (FMRL) at Florida State University as a Post-Doctoral Fellow. He joined the National Aerospace Laboratories in June 2000 and is currently Chief Scientist and Head of Experimental Aerodynamics Division. His main interests are in flow diagnostics, fluid mechanics and aeroacoustics. He has about 80 publications in international refereed journals and conferences in addition to numerous invited lectures in international conferences.

He is a reviewer, guest editor, on several peer-reviewed international journals and is currently also on the Editorial Advisory board of the Springer journal *Experiments in Fluids*.

He is an Associate Fellow of the American Institute of Aeronautics and Astronautics and has been awarded the Prof. Satish Dhawan Award for Young Engineers in 2011 in addition to the Best Innovation award from CSIR-NAL in 2013.